Pergamon

Solid State Communications, Vol. 95, No. 5, pp. 281–286, 1995
Elsevier Science Ltd
Printed in Great Britain

0038-1098(95)00275-8

0038-1098/95 $9.50+.00

SYNTHESIS OF CARBON NITRIDE FILMS BY MAGNETICALLY ROTATED ARC-PLASMA JET CHEMICAL VAPOR DEPOSITION

Tyan-Ywan Yen and Chang-Pin Chou

Department of Mechanical Engineering, National Chiao Tung University,
Hsinchu 30050, Taiwan, R.O.C.

(*Received* 23 *January* 1995; *accepted* 27 *March* 1995 *by A.H. MacDonald*)

Carbon Nitride films have been grown on nickel substrates by magnetically rotated arc-plasma jet chemical vapor deposition (CVD). These films were characterized by scanning electron microscopy (SEM), wavelength dispersive X-ray spectrometry (WDS) transmission electron microscopy (TEM), and Raman spectroscopy. Small grains (~0.1μm) as well as nanocrystallites found in the films were identified to be β–C_3N_4. Raman spectrum also confirmed the existence of β–C_3N_4 phase in the films through three pronounced Raman bands at low frequency as expected from the Hooke's law approximation.

Keywords: A. thin films, B. chemical synthesis, C. scanning and transmission electron microscopy, E. inelastic light scattering

1. Introduction

It has been predicted by theoretical calculation [1-2] that a metastable phase of β–C_3N_4, which has the same structure as β–Si_3N_4, will have an exceptional hardness comparable to or greater than that of diamond. Recently, considerable efforts have been made in an attempt to synthesize β–C_3N_4 by using different experimental techniques [3-15]. So far there have been only a few reports [13-16] that confirmed the synthesis of crystalline β–C_3N_4 by providing X-ray diffraction (XRD) or transmission electron diffraction (TED) patterns of their resulting materials. Yu et al. [13], using rf sputtering of a graphite target in a pure nitrogen ambient, grew crystalline particles which were believed to be β–C_3N_4 grains in the film deposited on Si (1 0 0) wafers. Niu et al. [14] claimed to have synthesized crystalline β–C_3N_4 using laser ablation of graphite combined with an atomic nitrogen beam. Notably, they have pointed out the importance of atomic nitrogen in the synthesis of carbon nitride. From the results of the formation of crystalline carbon nitride using argon-nitrogen plasma arc irradiating a graphite rod anode, Matsumoto et al. [15] found that their plasma arc mainly consisted of N atoms and CN radicals. Song et al. [16] have successfully prepared carbon nitride thin films by NH_3-ion-beam-assisted deposition. They emphasized that the chemical activities possessed by nitrogen atoms were crucial in the formation of β–C_3N_4.

It is therefore suggested that atomic nitrogen may play a major role in the growth of β–C_3N_4. Among possible experimental techniques that may be adopted in order to generate high flux of atomic nitrogen the method of arc-plasma jet seems to be a favorable choice. It has been successfully used in the past to prepare CVD diamond films at very high growth rates [17]. A key feature of diamond CVD is the necessity for copious amounts of atomic hydrogen [18]. Arcjet provides the elevated temperature needed to produce a large degree of dissociation of hydrogen and high gas velocity for large total flux. Similarly, the non-equilibrium synthesis of β–C_3N_4 may be achieved through spraying a plasma jet, containing the reactive carbon species and atomic nitrogen, onto a water-cooled substrate at high velocity. In the present paper, we report the possibility of the growth of β–C_3N_4 using a magnetically rotated arc-plasma jet. The structure and composition of the obtained films were

characterized by SEM, WDS, TEM, TED, and Raman spectroscopy.

2. Experimental details

A schematic diagram of the magnetically rotated arc-plasma jet CVD apparatus is shown in Fig. 1. An external magnetic field was provided by a water-cooled coil and mounted coaxially with the plasma torch. The maximum magnetic strength which could be obtained with our power supply was 1000 Gauss at the center of the coil. The plasma torch consisted of a 4.0 mm thoriated tungsten cathode and an anode nozzle. The anode ring, pressed into a water-cooled copper support, was made of pure graphite with inner diameter of 10.0 mm. This type of construction of the anode allowed exchange of the graphite anode within a few seconds. The entire plasma torch and substrate holder were installed in a vacuum chamber evacuated by a mechanical pump which established the necessary pressure and flow requirements for these experiments. The arc was struck between the cone-shaped cathode and the inside wall of the graphite anode and made to rotate around electrodes by $\mathbf{I} \times \mathbf{B}$ force (where $\mathbf{I}$ is the arc current and $\mathbf{B}$ is the external magnetic field strength). Premixed source gases, argon and nitrogen, were introduced into the annulus between the anode and cathode with a significant degree of swirl to stabilized the arc. The graphite anode was evaporated as a results of high power density arc spots rotating on it and acted as a carbon source. A unique feature of our plasma jet is the intensive mixing, with the help of gas swirling and magnetic rotating, of evaporated carbon species with atomic nitrogen produced by the arc.

The resulting plasma jet impinged on a mirror-polished polycrystalline nickel substrate which was glued onto a water-cooled copper substrate holder with a high conductive adhesive. The chamber was evacuated to 1×10^{-3} torr before the deposition. The flow rates were 8 *l/min* for the argon and 4 *l/min* for the nitrogen. The pressure in the chamber was 60 torr. The arc current was 50-60 A and the voltage was 70-80 V. After the plasma jet became stable, the substrate holder was moved up slowly toward the jet in order to start the synthesis of carbon nitride. The substrate temperature was measured by an optical pyrometer and maintained at approximately 800°C by varying the distance between the nozzle and substrate. All measurements described in the present paper were made on films deposited for 10 mins. The morphology of the films was studied using a Hitachi S-2500 scanning electron microscope, equipped with a Microspec WDX-3PC wavelength dispersive X-ray spectrometry for chemical analysis. The microstructure of the films were analyzed using TEM and Raman spectroscopy. The TEM image and transmission electron diffraction (TED) patterns were obtained using a Jeol JEM-2000FX scanning transmission electron microscope. Raman spectra were collected in the backscanning geometry using a micro Raman spectrometer from Renishaw.

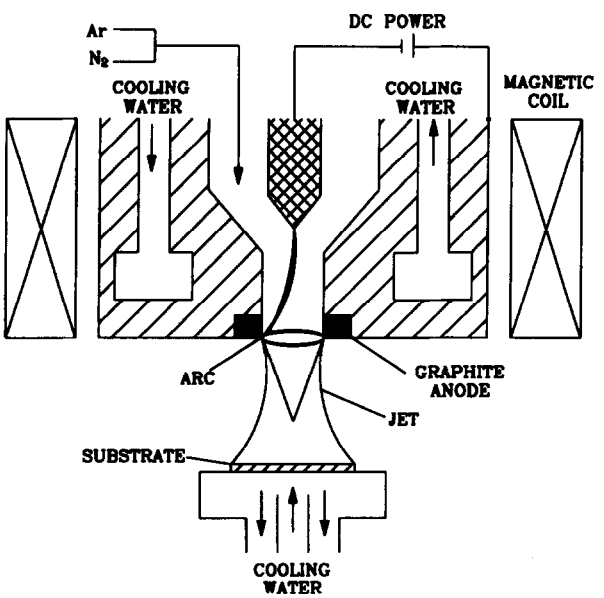

Fig. 1. Schematic diagram of the magnetically rotated arc-plasma jet CVD apparatus.

3. Results and discussion

The average composition of the films deposited on nickel substrates were obtained from WDS by measuring the nitrogen Kα and carbon Kα lines. B_4C and BN were chosen as standards for C and N respectively. The N-to-C concentration ratio in the films were estimated to be [N]/[C]=0.75 by using an appropriate matrix correction program. This ratio is as high as those films produced by other techniques [12]. The scanning electron micrograph revealing the surface morphology of a carbon nitride film is shown in Fig. 2. The micrograph shows that the film is composed of randomly distributed grains of ~0.1 μm size and aggregates of small grains. Quantitative determination of the composition of individual grain was difficult due to the limitation of electron-beam size and a large substrate effects.

TEM analysis was performed to investigate possible crystalline phases and microstructure in the obtained films.

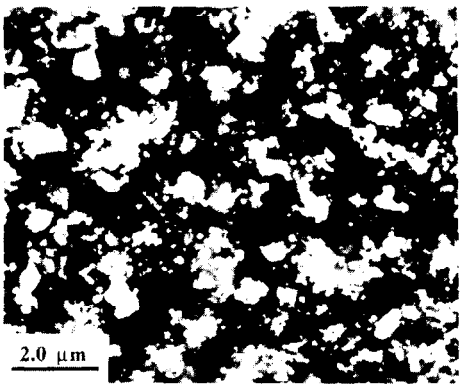

Fig. 2. Scanning electron micrograph of a carbon nitride film grown on a nickel substrate.

The specimens were prepared by directly scrapping carbon nitride films onto Cu grids. TEM bright-field and dark-field electron micrographs and its corresponding TED pattern are shown in Fig. 3. The ring pattern in Fig. 3(c) indicates that our film contains polycrystalline carbon nitride material. The lattice spacings were measured directly from the TED pattern and tabulated in Table 1. Significantly, both the peak positions and intensities of all the diffraction rings in the TED pattern match with the theoretical β–C_3N_4 pattern, with the exception of only two rings with very weak intensities. The rings which correspond to the β–C_3N_4 diffraction were indexed in Fig. 3(c). Assuming a hexagonal structure, the average lattice constants were also calculated to be a=6.35Å and c=2.48Å. To check this crystalline phase, a dark-field image, as shown in Fig. 3(b), was taken with a strong reflection spot marked by arrow in Fig. 3(c). The largest grain size observed in the dark-field micrograph is about 0.1 μm in diameter. Many randomly distributed tiny crystallites with grain sizes < 10 nm and clusters of grains are observed. This is consistent with the SEM observation. In recent reports [13-16], several important peaks in the calculated pattern of β–C_3N_4 are missing in the TED and XRD results. The (1 0 0), (1 1 0), (2 0 0), (1 1 1), and (3 0 0) reflections were calculated to be medium or strong and are either missing from or are weak in the reported diffraction patterns. Yu et al. [13] have observed β–C_3N_4 grains (0.5-1 μm) in the film deposited on Si (1 0 0), but they could only find these crystalline β–C_3N_4 particles near the film-substrate interface.

Indeed, these results indicate that our films contain a high fraction of crystalline β–C_3N_4 and this is mainly attributed to the arcjet technique employed. In viewing our plasma torch, the high dc-arc temperatures provide a

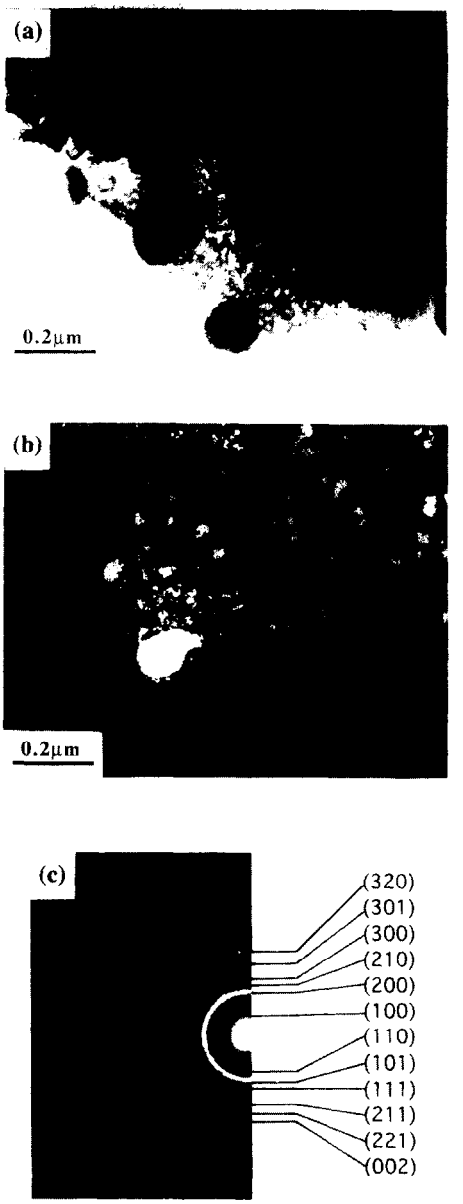

Fig. 3. (a) TEM bright-field micrograph of the carbon nitride film. (b) Dark-field micrograph taken with the reflection spot marked by arrow in (c). (c) The corresponding electron-diffraction pattern. The diffraction rings corresponding to the β–C_3N_4 phase are indexed in the figure.

source with high concentration of atomic nitrogen. Rotation of arc distributes the anode heat flux over a large area, therefore reducing non-evaporated larger carbon fragments to eject from graphite anode. Furthermore, a significant swirl in the plasma plume would promote the mixing to aid chemical reactions between evaporated carbon species and atomic nitrogen. Because of the high jet velocity, these reactive species are transported to the

Table 1. Comparison of the TED data from Fig. 3(c) with the calculated β–C_3N_4 powder-diffraction pattern. s, m, w, and vw represent strong, medium, weak, and very weak diffraction intensities.

calculated β–C_3N_4 pattern*			TED	
d(Å)	hkl	Intensity	d(Å)	Intensity
5.656	100	m	5.41	m
			3.63	vw
3.213	110	m	3.04	m
2.783	200	s	2.60	s
2.259	101	s	2.28	s
2.103	210	m	2.10	m
1.953	111	m	1.99	m
1.855	300	m	1.85	m
			1.66	vw
1.598	211	w	1.58	w
1.543	310	w		
1.481	301	w	1.47	m
1.345	221	w	1.37	w
1.277	320	w	1.26	m
1.229	002	w	1.21	vw

* Theoretical values [13]

substrate surface and subsequently quenched to generate a nonequilibrium composition plasma. Thus the formation of β–C_3N_4 is facilitated.

Raman spectroscopy is a useful tool for studying crystalline quality because of its sensitivity to slight variations in the lattice symmetry. Therefore, it is desirable to use Raman spectroscopy to characterize carbon nitride phases in all carbon- nitrogen films. Up to now, most of the Raman spectra reported for carbon nitride [6, 19-23] were similar to that for amorphous carbon films. The major features of these spectra are the G and D characteristic bands common to all disordered polycrystalline and noncrystalline graphitic carbons [24-25]. These two bands are approximately at 1580 cm^{-1} (G band) and 1355 cm^{-1} (D band) respectively. In contrast, Ren et al. [26] reported a Raman spectrum for their carbon nitride film, in which a high peak at 2190 cm^{-1} was observed and attributed to a triple bonded carbon-nitrogen stretching mode. On the other hand, Bousetta et al. [27] showed that the main peak in their Raman spectra, appeared at 1275 cm^{-1}, were associated with a fourfold coordinated carbon-nitrogen stretching mode. However, since β–C_3N_4 was proposed to adopt the crystal structure of β–Si_3N_4 [2], the Raman spectrum of β–C_3N_4 would be analogous to its β–Si_3N_4 counterpart.

An approach to estimate the Raman peaks for β–C_3N_4 has been suggested [6] (also refer to a footnote in Ref. 6) by correlating the stretching frequency for the carbon-nitrogen bond to the silicon-nitrogen bond through Hooke's law

$$\nu_{CN}/\nu_{SiN} = (B_{CN}\, d_{CN}\, u_{SiN} / B_{SiN} d_{SiN} u_{CN})^{1/2} \qquad (1)$$

where B is the bulk modulus, d is the bond length, and u is the reduced mass. A scale factor of 1.43 has been calculated by substituting the bulk moduli and bond lengths (for β–Si_3N_4, B = 256GPa, d = 1.74Å and for β–C_3N_4, B = 427GPa, d = 1.47Å) [2] into the Hooke's law approximation of Eq. (1). Wada et al. [28] employed group theory to study the Raman spectra of β–Si_3N_4 (space group C_{6h}^2) and yield the following results :

$$\Gamma_{optic} = 4A_g + 3B_g + 2E_{1g} + 5E_{2g} + 2A_u + 4B_u + 4E_{1u} + 2E_{2u} \qquad (2)$$

Of these the A_g, E_{1g} and E_{2g} modes are Raman active. Totally 11 Raman peaks were observed for a β–Si_3N_4 powder sample[28], of which three intense peaks at 186, 210 and 229 cm^{-1} were tentatively assigned to A_g modes. The analogous peaks for β–C_3N_4 are thus calculated and listed in Table 2. On the basis of the symmetry properties of the polarizability tensor α of different crystals, the direction of the electric vector **E** of the exciting radiation that permit the appearance of a Raman-active vibrational mode in the spectrum can be deduced from the equation $\mathbf{P}=\alpha \cdot \mathbf{E}$. All the totally symmetric vibrational mode in hexagonal crystal system (A_g mode in β–Si_3N_4) are the most commonly observed modes, because they appear in the Raman spectra without special requirement for the **E** direction. Therefore, the three pronounced A_g peaks are especially useful as a spectral signature in the Raman spectrum of β–Si_3N_4 [29]. Based on this, it is possible to interpret the Raman spectrum of β–C_3N_4.

Fig. 4 shows a typical Raman spectrum of the as-deposited films. The most striking feature in this spectrum is the fact that instead of the Raman G and D bands as well as diamond (1332 cm^{-1}) peak, two prominent bands are observed at about 300 cm^{-1}. This spectrum was analyzed using a curve fitting computer program in order to determine the intensities, peak positions, and linewidths of the individual Raman features. The results obtained by decomposing the experimental spectrum into five Lorentzian lines superimposed on a quadratic polynomial

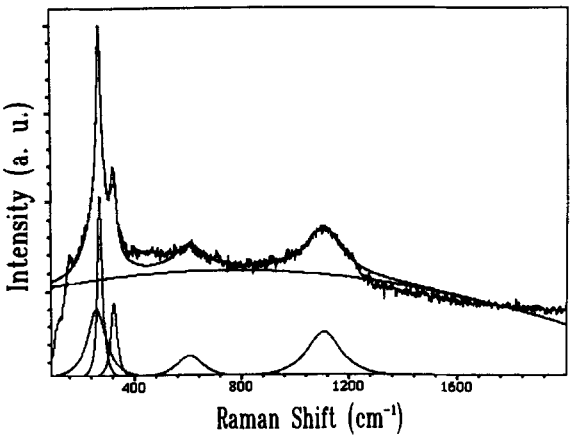

Fig. 4. Raman spectrum and computer decomposition from a carbon nitride film.

background (attributed to fluorescence) are displayed in Fig. 4 and the peak positions are tabulated in Table 2. Although only five peaks were used in the fit, the three intense bands appeared at 266, 280 and 330 cm^{-1} matched very well with the three A_g peaks calculated for β–C_3N_4 at 266, 300 and 327 cm^{-1}. The larger downshifting for one of the A_g modes and appreciable broadening for all peaks might be caused by the incorporation of some type of structural disorder into β–C_3N_4 crystals during the vapor deposition process. Small grain size, as shown by TEM, might also be responsible for the shifting and broadening of the Raman peaks, and the missing of some internal Raman modes. Nevertheless, the Raman spectrum provides unambiguous confirmation of the presence of β–C_3N_4 phase in our films.

Table 2. Experimental Raman peaks in β–Si_3N_4 and the calculated β–C_3N_4 lattice mode frequencies from the Hooke's law approximation (scale factor = 1.43). The Raman peak frequencies decomposed from the Raman spectrum shown in Fig. 4 are compared with the calculated β–C_3N_4 Raman frequencies.

β–Si_3N_4* Raman frequency(cm^{-1})	β–C_3N_4 Raman frequency(cm^{-1})		
observed	calculated	observed	Diff.(%)
144	206		
186	266	266	0.0
210	300	280	6.7
229	327	330	0.9
451	645	611	5.3
619	885		
732	1047	1110	6.0
865	1237		
928	1327		
939	1343		
1047	1497		

* Experimental data [28]

4. Conclusions

A new approach to carbon nitride films synthesis is presented. The major advantages of the magnetically rotated arc-plasma jet include the production of high reactive species fluxes and the intensive mixing of evaporated carbon species with atomic nitrogen. TEM and TED analyses gave strong evidence of the formation of crystalline β–C_3N_4 in the films deposited on nickel substrates. Raman spectrum also provides unambiguous confirmation of the presence of β–C_3N_4 phase through three pronounced Raman bands at low frequency as expected from the Hooke's law approximation.

Acknowledgments- This work was supported by the National Science Council, grant NSC84-2216-E-009-013, of R.O.C. We would like to thank Dr. Kuei-Hsien Chen for helpful discussion and use of Raman spectroscopy facility at Academic Sinica, Taipei.

References

1. A. Y. Liu and M. L. Cohen, Science 245, 841(1989).
2. A. Y. Liu and M. L. Cohen, Phys. Rev. B 41, 10727(1990).
3. J. J. Cuomo, P. A. Leary, D. Yu, W. Reuter, and M. Frisch, J. Vac. Sci. Technol. 16, 299(1979).
4. H. X. Han and B. J. Feldman, Solid State Commun. 65, 921(1988).
5. T. Sekine, H. Kanda, Y. Bando, M. Yokoyama, and K. Hojou, J. Mater. Sci. Lett. 9, 1376(1990).
6. M. Wixom, J. Am. Ceram. Soc. 73, 1973(1990).
7. M. Y. Chen, X. Lin, V. P. Dravid, Y. W. Chung, M. S. Wong, and W. D. Sproul, Surf. Coatings Technol. 54/55, 360(1992).
8. F. Fujimoto and K. Ogata, Jpn. J. Appl. Phys. 32, L420(1993).
9. S. Kumar and T. L. Transley, Solid State Commun. 88, 803(1993).

10. M. Diani, A. Mansour, L. Kubler, J. L. Bischoff, and D. Bolmont, Diamond Relat. Mater. 3, 264(1994).
11. A. Hoffman, I. Gouzman, and R. Brener, Appl. Phy. Lett. 64, 845(1994).
12. D. Marton, K. J. Boyd, A. H. Al-Bayati, S. S. Todorov, and J. W. Rabalais, Phys. Rev. Lett. 73, 118(1994).
13. K. M. Yu, M. L. Cohen, E. E. Haller, W. L. Hansen, A. Y. Liu, and I. C. Wu, Phys. Rev. B 49, 5034(1994).
14. C. Niu, Y. Z. Lu, and C. M. Lieber, Science 261, 334(1993).
15. O. Matsumoto, T. Kotaki, H. Shikano, K. Takemura, and S. Tanaka, J. Electrochem. Soc. 141, L16(1994).
16. H. W. Song, F. Z. Cui, X. M. He, W. Z. Li, and H. D. Li, J. Phys. : Condens. Matter. 6, 6125(1994).
17. N. Ohtake and M. Yoshikawa, J. Electrochem. Soc. 137, 717(1990).
18. K. Spear, J. Am. Ceram. Soc. 72, 171(1989).
19. J. H. Kaufman, S. Metin, and D. D. Saperstein, Phys. Rev. B 39, 13053(1989).
20. L. Maya, D. R. Cole, and E. W. Hagaman, J. Am. Ceram. Soc. 74, 1686(1991).
21. M. Y. Chen, D. Li, X. Lin, V. P. Dravid, Y. W. Chung, M. S. Wong, and W. D. Sproul, J. Vac. Sci. Technol. A11, 521(1993).
22. G. Mariotto, F. L. Freire, Jr., and C. A. Achete, Thin Solid Films 241,255(1994).
23. F. Rossi, B. Andre', A. Veen, P. E. Mijnarends, H. Schut, F. Labohm, H. Dunlop, M. P. Delplancke, and K. Hubbard, J. Mater. Res. 9, 2440(1994).
24. R. J. Nemanich and S. A. Solin, Phys. Rev. B 20, 392(1979).
25. R. O. Dillon and J. A. Woolam, Phys. Rev. B 29, 3482(1984).
26. Z. M. Ren, Y. C. Du, Z. F. Ying, Y. X. Qiu, X. X. Xiong, J. D. Wu, and F. M. Li, Appl. Phys. Lett. 65, 1361(1994).
27. A. Bousetta, M. Lu, A. Bensaoula, and A. Schultz, Appl. Phys. Lett. 65, 696(1994).
28. N. Wada, S. A. Solin, J. Wong, and S. Prochazka, J. Non-Cryst. Solids 43, 7(1981).
29. A. Takase and E. Tani, J. Mater. Sci. Lett. 6, 607(1987).